Clim. Past Discuss., 9, 1599–1625, 2013
www.clim-past-discuss.net/9/1599/2013/
doi:10.5194/cpd-9-1599-2013

Climate of the Past
Discussions
Open Access

Evaluating the dominant components of warming in Pliocene climate simulations

D. J. Hill[1,2], A. M. Haywood[1], D. J. Lunt[3], S. J. Hunter[1], F. J. Bragg[3], C. Contoux[4,5], C. Stepanek[6], L. Sohl[7], N. A. Rosenbloom[8], W.-L. Chan[9], Y. Kamae[10], Z. Zhang[11,12], A. Abe-Ouchi[9,13], M. A. Chandler[7], A. Jost[5], G. Lohmann[6], B. L. Otto-Bliesner[8], G. Ramstein[4], and H. Ueda[10]

[1]School of Earth and Environment, University of Leeds, Leeds, UK
[2]British Geological Survey, Keyworth, Nottingham, UK
[3]School of Geographical Sciences, University of Bristol, Bristol, UK
[4]Laboratoire des Sciences du Climat et de l'Environnement, Saclay, France
[5]Sisyphe, CNRS/UPMC Univ. Paris 06, Paris, France
[6]Alfred Wegener Institute Helmholtz Centre for Polar and Marine Research, Bremerhaven, Germany
[7]Columbia University – NASA/GISS, New York, NY, USA
[8]National Center for Atmospheric Research, Boulder, Colorado, USA
[9]Atmosphere and Ocean Research Institute, University of Tokyo, Kashiwa, Japan
[10]Graduate School of Life and Environmental Sciences, University of Tsukuba, Tsukuba, Japan
[11]UniResearch and Bjerknes Centre for Climate Research, Bergen, Norway

[12]Nansen-zhu International Research Centre, Institute of Atmospheric Physics, Chinese Academy of Sciences, Beijing, China
[13]Japan Agency for Marine-Earth Science and Technology, Yokohama, Japan

Received: 28 February 2013 – Accepted: 4 March 2013 – Published: 26 March 2013

Correspondence to: D. J. Hill (eardjh@leeds.ac.uk)

Published by Copernicus Publications on behalf of the European Geosciences Union.

Discussion Paper | Discussion Paper | Discussion Paper | Discussion Paper |

Abstract

The Pliocene Model Intercomparison Project is the first coordinated climate model comparison for a warmer palaeoclimate with atmospheric CO_2 significantly higher than pre-industrial concentrations. The simulations of the mid-Pliocene warm period show global warming of between 1.8 and 3.6 °C above pre-industrial surface air temperatures, with significant polar amplification. Here we perform energy balance calculations on all eight of the coupled ocean–atmosphere simulations within PlioMIP Experiment 2 to evaluate the causes of the increased temperatures and differences between the models. In the tropics simulated warming is dominated by greenhouse gas increases, with cloud albedo feedbacks enhancing the warming in most of the models, but by widely varying amounts. The responses to mid-Pliocene climate forcing in the Northern Hemisphere mid-latitudes are substantially different between the climate models, with the only consistent response being a warming due to increased greenhouse gases. In the high latitudes all the energy balance components become important, but the dominant warming influence comes from the clear sky albedo. This demonstrates the importance of specified ice sheet and high latitude vegetation boundary conditions and simulated sea ice and snow albedo feedbacks. The largest components in the overall uncertainty are associated with cloud albedo feedbacks in the tropics and polar clear sky albedo, particularly in sea ice regions. These simulations show that high latitude albedo feedbacks provide the most significant enhancements to Pliocene greenhouse warming.

1 Introduction

Atmospheric carbon dioxide concentrations continue to rise due to anthropogenic emissions. The latest measurements show that annual mean concentrations have risen beyond 390 parts per million (Conway et al., 2012). The Pliocene was the last period of Earth history with similar to modern atmospheric CO_2 concentrations (Seki et al., 2009;

Kürschner et al., 1996). These were associated with elevated global temperatures in both the ocean (Dowsett et al., 2012) and on land (Salzmann et al., 2013). As the last period of global warmth before the climate transition into the bipolar ice age cycles of the Pleistocene, the mid-Pliocene warm period (mPWP) has been a target for both palaeoenvironmental data acquisition and palaeoclimate modelling over a number of years (Dowsett et al., 1992, 2010; Chandler et al., 1994; Haywood et al., 2009). Although a number of different General Circulation Models (GCMs) have been used to simulate Pliocene climates (Chandler et al., 1994; Sloan et al., 1996; Haywood et al., 2000, 2009), it is only recently that a coordinated multi-model experiment has been initiated, with standardized design for mid-Pliocene simulations (Haywood et al., 2010, 2011).

The Pliocene Model Intercomparison Project (PlioMIP) represents the first coordinated multi-model experiment to simulate a warmer than modern palaeoclimate, with high atmospheric CO_2 concentrations (405 ppmv). It has recently been added to the Paleoclimate Model Intercomparison Project (PMIP; Hill et al., 2012) and the first phase, incorporating two simulations, completed. This paper focuses on PlioMIP Experiment 2, designed for coupled ocean-atmosphere General Circulation Models (GCMs; Haywood et al., 2011). Although, many of the large scale features of the simulated Pliocene climate have been well documented (Dowsett et al., 2012; Haywood et al., 2013; Salzmann et al., 2013; R. Zhang et al., 2013; Z. Zhang et al., 2013a, b), the causes of the simulated changes and differences between the simulations have not been extensively explored prior to this study. In this paper the energy balance of the PlioMIP Experiment 2 simulations are analysed in order to understand the causes of Pliocene atmospheric warming and the latitudinal distribution of increased surface air temperatures.

2 Participating models

Eight different modelling groups have submitted simulations to PlioMIP Experiment 2. All of these models are coupled ocean-atmosphere GCMs, but range in complexity and spatial resolution. Table 1 contains the details of each of the models' simulation, including the resolution at which it was run, the boundary conditions employed and the model initialization. Each of the simulations is documented in much more detail in a separate paper within a special issue of Geoscientific Model Development, referenced in Table 1. The general climate sensitivity of the model and the annual mean global warming produced in its PlioMIP Experiment 2 simulation is detailed in Table 2. Further details about the models can also be found in Haywood et al. (2013) and the references therein.

3 PlioMIP experiment 2

PlioMIP uses the latest iteration of the PRISM (Pliocene Research, Interpretation and Synoptic Mapping) mid-Pliocene palaeoenvironmental reconstruction, PRISM3 (Dowsett et al., 2010), as the basis for the imposed model boundary conditions. This reconstruction represents the peak averaged warm climate of the mid-Pliocene warm period (mPWP; 3.246–3.025 Ma; Dowsett et al., 2010) in the middle of the Piacenzian Stage. It incorporates sea surface temperatures, bottom water temperatures (Dowsett et al., 2009), vegetation (Salzmann et al., 2008), ice sheets (Hill et al., 2007, 2010), orography (Sohl et al., 2009) and a global land-sea mask equivalent to 25 m of sea level rise. The vegetation, ice sheets and orographic reconstructions are all required as boundary conditions within the models, although they must be translated onto the resolution of each individual model. Vegetation was reconstructed using the BIOME4 classification scheme (Kaplan, 2001) and must therefore be translated onto the vegetation scheme used by each model.

Although as part of PlioMIP a standard experimental design was implemented, it was appreciated that not all of the modelling groups would be able to perform the ideal mPWP experiment. As such, alternate boundary conditions were specified for those models that could not effectively change the land-sea mask from the present-day configuration. This meant that the ocean advance specified in low-lying coastal regions and West Antarctica as well as the filling of Hudson Bay were not included in some of the simulations (Table 1). Furthermore a choice was given concerning the initial state of the ocean between a specification of the PRISM3 three-dimensional ocean temperatures (Dowsett et al., 2009) and initialization with the same ocean temperatures as the pre-industrial control simulation (Haywood et al., 2011).

4 PlioMIP experiment 2 global warming

Overall the PlioMIP models simulate mPWP annual mean global surface air temperature (SAT) increases of 1.8–3.6 °C (Table 2). Tropical temperatures increased by only 1.0–3.1 °C, while in the Arctic surface air temperatures increased by 3.5–13.2 °C (Fig. 1b). Sea surface temperatures (SSTs) follow a similar pattern, but with a reduced magnitude of global warming and significantly greater warming in the North Pacific (Fig. 1d). The patterns of warming in the northern mid-latitudes and southern high latitudes are much more variable between the different models. Relative variation between the models peaks in the North Atlantic, mid-latitude mountain regions and central Antarctica for SATs (Fig. 1c) and in the North Atlantic, North Pacific and sea ice areas of the Arctic and Southern Oceans for SSTs (Fig. 1f).

The warming of the PlioMIP simulations is accompanied by increased precipitation (Haywood et al., 2013) and monsoonal activity (R. Zhang et al., 2013) and reductions in sea ice (Clark et al., 2013), although the Atlantic Meridional Overturning Circulation shows little response (Z. Zhang et al., 2013b). Global mean temperature response (Table 2), as well as polar amplification (Salzmann et al., 2013), do not show a strong correlation to either the use of preferred or alternate boundary conditions or to the initial

conditions of the ocean. This gives us some confidence that these choices within the experimental design do not dominate the warming signal.

5 Energy balance approach

Energy balance analyses have been used in many palaeoclimate simulations and ensembles to understand the simulated temperature changes (e.g. Donnadieu et al., 2006; Murakami et al., 2008). The results from each of the GCMs can be broken down in to the various components in the energy balance of each individual simulation. The approach taken builds on the energy balance modelling of Heinemann et al. (2009) and Lunt et al. (2012), where globally averaged temperatures are approximated using planetary albedo α and the effective longwave emissivity ε.

$$\frac{S_0}{4}(1-\alpha) = \varepsilon\sigma T^4$$

Where S_0 is the total solar irradiance (1367 $\mathrm{W\,m^{-2}}$) and σ is the Stefan-Boltzmann constant ($5.67\times10^{-8}\,\mathrm{W\,m^{-2}\,K^{-4}}$). Planetary albedo is the ratio of outgoing (↑) to incoming (↓) shortwave radiation at the top of the atmosphere (TOA) and effective longwave emissivity the ratio of TOA to surface (SURF) upward longwave radiation,

$$\alpha = \frac{\mathrm{SW}^{\uparrow}_{\mathrm{TOA}}}{\mathrm{SW}^{\downarrow}_{\mathrm{TOA}}}, \varepsilon = \frac{\mathrm{LW}^{\uparrow}_{\mathrm{TOA}}}{\mathrm{LW}^{\uparrow}_{\mathrm{SURF}}}$$

This can be expanded to approximate the one dimensional, zonally averaged temperatures at each latitude of the model grid by including a component for the implied net meridional heat transport divergence (H).

$$\mathrm{SW}^{\downarrow}_{\mathrm{TOA}}(1-\alpha) - H = \varepsilon\sigma T^4$$

Where

$$H = (\mathrm{SW}^{\downarrow}_{\mathrm{TOA}} - \mathrm{SW}^{\uparrow}_{\mathrm{TOA}}) - \mathrm{LW}^{\uparrow}_{\mathrm{TOA}}$$

Thus the temperature at each latitude in a GCM experiment is given by:

$$T = \frac{(\mathrm{SW}^{\downarrow}_{\mathrm{TOA}}(1-\alpha) - H)^{1/4}}{\varepsilon\sigma} \equiv T(\varepsilon,\alpha,H)$$

By applying the notation of Lunt et al. (2012) to denote the pre-industrial control experiment as a second experiment represented by an apostrophe, the Pliocene surface air temperature warming (ΔT) can be calculated by:

$$\Delta T = T(\varepsilon,\alpha,H) - T(\varepsilon',\alpha',H')$$

Due to their small changes relative to their absolute values, Pliocene warming can be approximated by a linear combination of changes in emissivity (ΔT_ε), albedo (ΔT_α) and heat transport (ΔT_H). However, these components can be further broken down into the impact of changes in atmospheric greenhouse gases ($\Delta T_{\mathrm{gg}\varepsilon}$), clouds (on both emissivity; $\Delta T_{\mathrm{c}\varepsilon}$ and albedo; $\Delta T_{\mathrm{c}\alpha}$) and clear sky albedo ($\Delta T_{\mathrm{cs}\alpha}$; generally dominated by changes in surface albedo, but including atmospheric absorption and scattering components). In experiments and latitudes where changes in topography occur between the Pliocene and pre-industrial, the impact of these changes in surface altitude (ΔT_{topo}) must also be accounted for.

$$\Delta T = \Delta T_{\mathrm{gg}\varepsilon} + \Delta T_{\mathrm{c}\varepsilon} + \Delta T_{\mathrm{c}\alpha} + \Delta T_{\mathrm{cs}\alpha} + \Delta T_\mathrm{H} + \Delta T_{\mathrm{topo}}$$

Each of these components can be calculated from various combinations of Pliocene and pre-industrial albedos, emissivities and implied heat transports, although some

must be calculated in the clear sky case (denoted with a subscript cs).

$$\Delta T_{gg\varepsilon} = T(\varepsilon_{cs}, \alpha_{cs}, H_{cs}) - T(\varepsilon'_{cs}, \alpha_{cs}, H_{cs}) - \Delta T_{topo}$$
$$\Delta T_{c\varepsilon} = (T(\varepsilon, \alpha, H) - T(\varepsilon_{cs}, \alpha, H)) - (T(\varepsilon', \alpha', H') - T(\varepsilon'_{cs}, \alpha', H'))$$
$$\Delta T_{c\alpha} = (T(\varepsilon, \alpha, H) - T(\varepsilon, \alpha_{cs}, H)) - (T(\varepsilon', \alpha', H') - T(\varepsilon', \alpha'_{cs}, H'))$$
$$\Delta T_{cs\alpha} = T(\varepsilon_{cs}, \alpha_{cs}, H_{cs}) - T(\varepsilon_{cs}, \alpha'_{cs}, H_{cs})$$
$$\Delta T_{H} = T(\varepsilon, \alpha, H) - T(\varepsilon, \alpha, H')$$

Although lapse rates vary over time and space, the impact of changing the topography in the Pliocene simulations (ΔT_{topo}) can be approximated by multiplying the change in topography (Δh) by a constant atmospheric lapse rate ($\gamma \approx 5.5\,\mathrm{K\,km^{-1}}$; Yang and Smith, 1985).

$$\Delta T_{topo} = \Delta h \cdot \gamma$$

6 Energy balance results for individual simulations

The energy balance calculations for each of the individual simulations within the PlioMIP Experiment 2 ensemble are shown in Fig. 2. The overall structure of the energy balance components is largely the same between all the simulations. However, there are large changes in the magnitude of impacts, many regional temperature changes and different relative contributions from the components for each simulation. Examination of the energy balance for the individual simulations within the PlioMIP Experiment 2 ensemble will enable us to understand these similarities and differences when the multi-model means and individual components are analysed.

The CCSM4 mPWP simulation shows a smaller global annual mean warming than most in the ensemble and less polar amplification. In the tropics and Southern Hemisphere mid-latitudes zonal mean warming of at least 1 °C is almost entirely greenhouse gas driven, with the very small temperature responses from the other components

cancelling out (Fig. 2a). In the northern mid-latitudes greenhouse warming still dominates, but significant contributions are also made by clear sky albedo and, at around 60° N, meridional heat transport. In northern high-latitudes both greenhouse gases and clear sky albedo have a large warming impact, although cloud albedo cooling provides a significant offset to the overall warming. In the Southern Hemisphere high-latitudes warming peaks over the Southern Ocean and over Antarctica at 75° S. Clear sky albedo drives warming over the Southern Ocean, from changes in modelled sea-ice, whilst being offset by changes in meridional heat transport and cloud albedo. Over the Antarctic, small warming from all the components, apart from cloud albedo (topography, cloud emissivity, greenhouse gas emissivity, clear sky albedo and implied heat transport), add up to give the largest zonally averaged warming in the CCSM4 simulation.

COSMOS is the warmest model in the PlioMIP ensemble, both in terms of its general climate sensitivity and also in its annual mean mid-Pliocene warming (Table 2). In the tropics and mid-latitudes greenhouse gas warming is generally reinforced by a significant warming due to cloud albedo (Fig. 2b). In the Arctic all the components show an amplified temperature response, although overall cloud impacts and heat transport contribute little to the warming compared to clear sky albedo and greenhouse gas warming. The Antarctic warming shows a similar response, although the cooling impact of cloud albedo is more prevalent.

GISS-E2-R has the lowest climate sensitivity in the PlioMIP ensemble, but its simulated Pliocene annual mean warming is greater than three of the other models. Simulated tropical and mid-latitude warming is close to that of greenhouse gases alone, but at many latitudes this is due to the significant temperature impacts of the other components largely cancelling out (Fig. 2c). High-latitude warming is dominated by clear sky albedo and greenhouse gases, but cloud albedo provides a significant negative feedback, particularly in the Arctic.

The simulations run using HadCM3 show one of the largest tropical temperature increases (along with the COSMOS simulations) of around 3 °C. This is produced via greenhouse gas forcing, enhanced by cloud albedo feedbacks (Fig. 2d). This warming

extends into the Northern Hemisphere mid-latitudes, but is reduced in the Southern Hemisphere mid-latitudes, as the impact of clouds is much reduced. Peak Arctic warming occurs at the latitudes of the modern sea ice limit, largely driven by changes in clear sky albedo. This impact drops of dramatically in the high Arctic, but is compensated for by increased warming due to heat transport and a reduction in cloud albedo cooling. In the Antarctic the clear sky albedo dominates the strong warming signal, but all of the factors have a significant impact.

Although the IPSL simulations show relatively subdued overall warming of 1 °C in the tropics and mid-latitudes, changes in clouds have a greater impact than in most PlioMIP simulations with similar magnitudes of warming (Fig. 2e). Greenhouse gases and cloud albedo warm the climate, while this is somewhat offset by cooling due to cloud emissivity. At high-latitudes strong clear sky albedo warming dominates the signal, but is associated with significant cooling from cloud albedo and reductions in meridional heat transport.

Tropical and mid-latitude warming in the MIROC simulations, one of the warmest on the ensemble, is dominated by greenhouse gas emissivity. However, the simulations show large regional warming from cloud albedo, at about 15° S, clear sky albedo, between 15 and 40° N, and meridional heat transport, at 45 to 60° S. High-latitude warming is dominated by clear sky albedo warming, only partially offset by cloud albedo changes. In the Arctic significant cooling also comes from changes in implied heat transport.

MRI-CGCM 2.3 has the smallest global annual mean warming of any of the PlioMIP Experiment 2 simulations (Table 2), despite having an average climate sensitivity. Tropical and mid-latitude warming is equivalent to that from greenhouse gases alone (Fig. 2g). Only in the Northern Hemisphere tropics and mid-latitudes do other factors play a significant role with the impacts of clear sky albedo and meridional heat transport offsetting each other. In the Northern Hemisphere tropics warming due to clear sky albedo is offset by cooling from changes in meridional heat transport. In mid-latitudes the impacts switch with cooling from clear sky albedo and warming from meridional

heat transport. At high-latitudes strong clear sky albedo warming is partially offset by cloud albedo cooling.

In the NorESM-L simulations Southern Hemisphere tropics and mid-latitutes warming is dominated by greenhouse gas emissivity, enhanced by cloud albedo (Fig. 2h). Cloud emissivity and meridional heat transport seem to have opposite but variable effects largely cancelling each other out. The Northern Hemisphere tropics and mid-latitudes show clear sky albedo enhancing the greenhouse gas warming. Cloud albedo feedbacks cool the tropics, but warm the mid-latitudes. The transition between mid-latitude and Arctic warming is particularly marked in NorESM-L, with strong greenhouse gas and clear sky albedo warming leading to the largest zonal mean warming in the PlioMIP Experiment 2 ensemble.

7 PlioMIP experiment 2 energy balance

In order to evaluate the simulation of warm climates of the Pliocene in general, a simple mean of the energy balance components from each of the individual simulations within the PlioMIP Experiment ensemble has been performed. When combined with the range of values within the ensemble this allows an assessment of the general cause of warming within the PlioMIP simulations and the robustness of any conclusion that can be drawn. Figure 3 shows the ensemble mean of the various energy balance components along with the range from the eight simulations, while Fig. 4 shows the individual energy balance components for each of the PlioMIP simulations.

Clear sky albedo includes contributions from surface albedo changes and atmospheric absorption and scattering. The latter could become important, even in models with no mechanisms for changing atmospheric transparency, as atmospheric thickness can increase due to changes in surface altitude. In the PlioMIP simulations clear sky albedo shows little contribution to warming in the tropics and Southern Hemisphere mid-latitudes. In the Northern Hemisphere mid-latitudes most models show a warming due to clear sky albedo, apart from the MRI-CGCM 2.3 simulation that shows a cooling

(Fig. 4a). In the polar regions, all the simulations show a strong warming signal from clear sky albedo, although the range in the magnitude of this warming is large. Changes in clear sky albedo mostly reflect changes on the Earth surface. Vegetation, snow and ice (both terrestrial ice masses and sea ice) are generally the main contributors to these changes. The warming found in the Northern Hemisphere, from 15–60° N is largely being driven by changes in the vegetation boundary conditions, particularly over the Sahara, Arabia and central Asia (Fig. 5). In the Arctic, warming due to clear sky albedo is primary driven by changes in ice sheet boundary conditions (reduced Greenland Ice Sheet) and changes in the predicted sea ice, but also by the poleward shift of the Arctic tree line (Salzmann et al., 2008). In the Southern Ocean and Antarctica the warming due to clear sky albedo has a double peak in most models, reflecting a reduction in the simulated Southern Ocean sea ice and a reduction in the prescribed Antarctic Ice Sheet.

All the simulations show a warming due to greenhouse gas emissivity of around 1–2 °C. These impacts are largely constant across latitudes, but with a slight polar amplification, especially in the Arctic (Fig. 4b). This is consistent with the prescribed increases in CO_2 (at 405 ppm for the mid-Pliocene, as opposed to 280 ppm in the pre-industrial simulations). The amplified high-latitude response is due to increases in the atmospheric water vapour predicted by the models. Differences in the simulation of this water vapour increase between different models explain why the range of temperature increases due to greenhouse gas warming is much higher in the polar regions. There are some suggestions of a similar increase in the tropical Northern Hemisphere, but the impact here is small.

The impacts of cloud albedo are small in the tropics and mid-latitudes. Different models seem to produce significantly different responses making the signal particularly noisy (Fig. 4c). However, the multi-model mean cloud albedo warming appears to reflect some of the large scale features of the PlioMIP simulations (Haywood et al., 2013). Between the equator and ∼45° there is a general warming due to a reduction in cloud albedo, interrupted by a cooling in the Northern Hemisphere tropics. This

cooling is due to an increase in cloud cover resulting from a northward shift of the Inter-Tropical Convergence Zone. In the high latitudes a significant increase in clouds leads to a significant cooling due to cloud albedo, peaking at between 3 and 6 °C in both hemispheres. Cloud emissivity shows a similar pattern of impacts, but in the opposite direction. However, the response is generally of a smaller magnitude (Fig. 4d), suggesting that, at least in these simulations, the primary cloud feedback on climate is through changes in planetary albedo.

Reconstruction of mid-Pliocene sea surface temperatures has led to increased heat transport in the North Atlantic being suggested as a primary driver of warming in the mid-Pliocene (Dowsett et al., 1992; Raymo et al., 1996). However, the implied overall meridional heat transport in the PlioMIP simulations, which integrates both oceanic and atmospheric transports, show little coherent signal. The fact that there is only one region where all of the simulations show a temperature change of the same direction suggests that the only robust conclusion that can be drawn about heat transport is a reduction of overall transport into the Arctic (Fig. 4e). This would be an expected result of polar amplification in the Arctic region under climate warming. These energy balance calculations support analysis of the Atlantic Meridional Overturning Circulation in the PlioMIP ensemble, which shows that there is little change in the northward heat transport in the North Atlantic (Z. Zhang et al., 2013b). This calls into question the role of ocean heat transport in the general warming of the mid-Pliocene. However, it may be important in the Pliocene variability of sea surface temperatures, which is particularly high in the North Atlantic (Dowsett et al., 2012).

8 Conclusions

The mid-Pliocene was probably the last time in Earth history when atmospheric carbon dioxide concentrations were similar to today (Seki et al., 2009; Kürschner et al., 1996). It has been the focus of palaeoenvironmental reconstructions and palaeoclimate model experiments for many years. However, the recently begun Pliocene Model

Intercomparison Project is the first time that coordinated multi-model experiments, with common boundary conditions and experimental protocols, have been undertaken. The warming seen in the Pliocene has been well documented from a wide variety of sites from across the globe and using a number of different proxy techniques (Dowsett et al., 2012; Salzmann et al., 2013). Previous simulations of Pliocene warmth have been performed with only a single model and multi-model analyses have been severely hampered by differing experimental designs (Haywood et al., 2009). For the first time a robust analysis of the causes of warming in Pliocene climate models is possible.

Energy balance calculations show that the tropical warming seen in all the models is primarily caused by greenhouse gas emissivity, with specified increases in atmospheric CO_2 concentration being the most important factor. Along with different sensitivity to the imposed CO_2 concentrations, changes in warming due to cloud albedo drive differences between the models in the tropics. At polar latitudes all the energy balance components become important, but clear sky albedo is the dominant driver of the high levels of warming and polar amplification. This is largely due to reductions in the specified ice sheets and simulated sea ice, but in the Northern Hemisphere also reflects a northward shift in the treeline. The models show very different response in the mid-latitudes of the Northern Hemisphere, with large uncertainties in the relative contributions of the different energy balance components. This is particularly true for the North Atlantic and Kuroshio Current regions, where intermodel variability is highest (Haywood et al., 2013). A more complete picture of these currents, their strength and variability within the Pliocene, would enable a much better analysis of the skill of the models in these key regions.

This energy balance analysis has shown some important features of the climate of the Pliocene. Atmospheric CO_2 concentrations remain controversial in the Pliocene, with significant uncertainties remaining. As tropical warming is largely driven by this factor, then simulations with particularly good representation of low latitude clouds could provide some new insight into the levels of CO_2 required to produce Pliocene climates. Similarly, accurate reconstructions of surface temperatures and atmospheric CO_2 in

combination with modelling studies could reveal the extent of changes to tropical cloud cover in the warmer Pliocene world.

Particularly strong warming in the high latitudes is driven by albedo feedbacks, especially from sea ice, ice sheets and vegetation. This is the region with the largest warming signal and also the largest uncertainties between the simulations. Therefore, improvements in the reconstruction of global ice cover and Arctic vegetation, along with improved data to evaluate the simulation of sea ice and high Arctic atmospheric and ocean temperatures, could significantly improve the simulations and allow much better constraints on total Pliocene warming. From the PlioMIP Experiment 2 simulations it appears that higher CO_2 concentrations warmed the planet and drove large surface albedo feedbacks in the high latitudes through changes in sea ice, vegetation and ice sheets. The latter two of these factors are important components of long term Earth system sensitivity, suggesting that long term response to CO_2 increases is greater than climate sensitivity (Lunt et al., 2010; Haywood et al., 2013).

Acknowledgements. D. J. H. acknowledges the Leverhulme Trust for the award of an Early Career Fellowship and the National Centre for Atmospheric Research and the British Geological Survey for financial support. A. M. H. and S. J. H. acknowledge that the research leading to these results has received funding from the European Research Council under the European Union's Seventh Framework Programme (FP7/2007-2013)/ERC grant agreement no. 278636. A. M. H. acknowledges funding received from the Natural Environment Research Council (NERC Grant NE/I016287/1, and NE/G009112/1 along with D. J. L). D. J. L and F. J. B. acknowledge NERC grant NE/H006273/1. D. J. L. acknowledges Research Councils UK for the award of an RCUK fellowship and the Leverhulme Trust for the award of a Phillip Leverhulme Prize. The HadCM3 simulations were carried out using the computational facilities of the Advanced Computing Research Centre, University of Bristol – http://www.bris.ac.uk/acrc/. G. L. received funding through the Helmholtz research programme PACES and the Helmholtz Climate Initiative REKLIM. C. S. acknowledges financial support from the Helmholtz Graduate School for Polar and Marine Research and from REKLIM. Funding for L. S. and M. C. provided by NSF Grant ATM0323516 and NASA Grant NNX10AU63A. B. L. O. and N. A. R. recognise that NCAR is sponsored by the US National Science Foundation (NSF) and computing resources were provided by the Climate Simulation Laboratory at NCAR's Computational and

Information Systems Laboratory (CISL), sponsored by the NSF and other agencies. W.-L. C. and A. A.-O. would like to thank the Japan Society for the Promotion of Science for financial support and R. Ohgaito for advice on setting up the MIROC4m experiments on the Earth Simulator, JAMSTEC. The source code of MRI model is provided by S. Yukimoto, O. Arakawa, and A. Kitoh in Meteorological Research Institute, Japan. Z. Z. acknowledges that the development of NorESM-L was supported by the Earth System Modelling (ESM) project funded by Statoil, Norway. Aisling Dolan is acknowledged for a beautiful title for this paper.

References

Bragg, F. J., Lunt, D. J., and Haywood, A. M.: Mid-Pliocene climate modelled using the UK Hadley Centre Model: PlioMIP Experiments 1 and 2, Geosci. Model Dev., 5, 1109–1125, doi:10.5194/gmd-5-1109-2012, 2012.

Chan, W.-L., Abe-Ouchi, A., and Ohgaito, R.: Simulating the mid-Pliocene climate with the MIROC general circulation model: experimental design and initial results, Geosci. Model Dev., 4, 1035–1049, doi:10.5194/gmd-4-1035-2011, 2011.

Chandler, M., Rind, D., and Thompson, R.: Joint investigations of the middle Pliocene climate II: GISS GCM Northern Hemisphere results, Global Planet. Change, 9, 197–219, 1994.

Clark, N. A., Williams, M., Hill, D. J., Quilty, P., Smellie, J., Zalasiewicz, J., Leng, M., and Ellis, M.: Fossil proxies of climate and seasonality from the late Neogene Antarctic shelf, Naturwissenschaften, submitted, 2013.

Contoux, C., Ramstein, G., and Jost, A.: Modelling the mid-Pliocene Warm Period climate with the IPSL coupled model and its atmospheric component LMDZ5A, Geosci. Model Dev., 5, 903–917, doi:10.5194/gmd-5-903-2012, 2012.

Conway, T. J., Lang, P. M., and Masarie, K. A.: Atmospheric carbon dioxide dry air mole fractions from the NOAA ESRL Carbon Cycle Cooperative Global Air Sampling Network, 1968–2011, Version: 2012-08-15, available at: ftp://ftp.cmdl.noaa.gov/ccg/co2/flask/event/ (last access: 20 March 2013), 2012.

Donnadieu, Y., Pierrehumbert, R., Jacob, R., and Fluteau, F.: Modelling the primary control of paleogeography on Cretaceous climate, Earth Planet. Sci. Lett., 248, 426–437, 2006.

Dowsett, H. J., Cronin, T. M., Poore, R. Z., Thompson, R. S., Whatley, R. C., and Wood, A. M.: Micropaleontological evidence for increased meridional heat transport in the North Atlantic Ocean during the Pliocene, Science, 258, 1133–1135, 1992.

Dowsett, H. J., Robinson, M. M., and Foley, K. M.: Pliocene three-dimensional global ocean temperature reconstruction, Clim. Past, 5, 769–783, doi:10.5194/cp-5-769-2009, 2009.

Dowsett, H. J., Robinson, M., Haywood, A. M., Salzmann, U., Hill, D. J., Sohl, L., Chandler, M. A., Williams, M., Foley, K., and Stoll, D.: The PRISM3D paleoenvironmental reconstruction, Stratigraphy, 7, 123–139, 2010.

Dowsett, H. J., Robinson, M. M., Haywood, A. M., Hill, D. J., Dolan, A. M., Stoll, D. K., Chan, W. L., Abe-Ouchi, A., Chandler, M. A., Rosenbloom, N. A., Otto-Bleisner, B. L., Bragg, F. J., Lunt, D. J., Foley, K. M., and Riesselman, C. R.: Assessing confidence in Pliocene sea surface temperatures to evaluate predictive models, Nature Climate Change, 2, 365–371, 2012.

Haywood, A. M., Valdes, P. J., and Sellwood, B. W.: Global scale palaeoclimate reconstruction of the middle Pliocene climate using the UKMO GCM: initial results, Global Planet. Change, 25, 239–256, 2000.

Haywood, A. M., Chandler, M. A., Valdes, P. J., Salzmann, U., Lunt, D. J., and Dowsett, H. J.: Comparison of mid-Pliocene climate predictions produced by the HadAM3 and GCMAM3 general circulation models, Global Planet. Change, 66, 208–224, doi:10.1016/j.gloplacha.2008.12.014, 2009.

Haywood, A. M., Dowsett, H. J., Robinson, M. M., Stoll, D. K., Dolan, A. M., Lunt, D. J., Otto-Bliesner, B., and Chandler, M. A.: Pliocene Model Intercomparison Project (PlioMIP): experimental design and boundary conditions (Experiment 2), Geosci. Model Dev., 4, 571–577, doi:10.5194/gmd-4-571-2011, 2011.

Haywood, A. M., Hill, D. J., Dolan, A. M., Otto-Bliesner, B. L., Bragg, F., Chan, W.-L., Chandler, M. A., Contoux, C., Dowsett, H. J., Jost, A., Kamae, Y., Lohmann, G., Lunt, D. J., Abe-Ouchi, A., Pickering, S. J., Ramstein, G., Rosenbloom, N. A., Salzmann, U., Sohl, L., Stepanek, C., Ueda, H., Yan, Q., and Zhang, Z.: Large-scale features of Pliocene climate: results from the Pliocene Model Intercomparison Project, Clim. Past, 9, 191–209, doi:10.5194/cp-9-191-2013, 2013.

Heinemann, M., Jungclaus, J. H., and Marotzke, J.: Warm Paleocene/Eocene climate as simulated in ECHAM5/MPI-OM, Clim. Past, 5, 785–802, doi:10.5194/cp-5-785-2009, 2009.

Hill, D. J., Haywood, A. M., Hindmarsh, R. C. M., and Valdes, P. J.: Characterizing ice sheets during the Pliocene: evidence from data and models, in: Deep-Time Perspectives on Climate Change: Marrying the signal from Computer Models and Biological Proxies, edited by: Williams, M., Haywood, A. M., Gregory, F. J., and Schmidt, D. N., The Micropalaeontological Society, Special Publications, The Geological Society, London, 517–538, 2007.

Hill, D. J., Dolan, A. M., Haywood, A. M., Hunter, S. J., and Stoll, D. K.: Sensitivity of the Greenland Ice Sheet to Pliocene sea surface temperatures, Stratigraphy, 7, 111–122, 2010.

Kamae, Y. and Ueda, H.: Mid-Pliocene global climate simulation with MRI-CGCM2.3: set-up and initial results of PlioMIP Experiments 1 and 2, Geosci. Model Dev., 5, 793–808, doi:10.5194/gmd-5-793-2012, 2012.

Kaplan, J. O.: Geophysical Applications of Vegetation Modeling, Ph.D. Thesis, Lund University, Lund, 2001.

Kürschner, W. M., van der Burgh, J., Visscher, H., and Dilcher, D. L.: Oak leaves as biosensors of late Neogene and early Pleistocene paleoatmospheric CO_2 concentrations, Mar. Micropalaeontol., 27, 299–312, 1996.

Lunt, D. J., Haywood, A. M., Schmidt, G. A., Salzmann, U., Valdes, P. J., and Dowsett, H. J.: Earth system sensitivity inferred from Pliocene modelling and data, Nat. Geosci., 3, 60–64, 2010.

Lunt, D. J., Dunkley Jones, T., Heinemann, M., Huber, M., LeGrande, A., Winguth, A., Loptson, C., Marotzke, J., Roberts, C. D., Tindall, J., Valdes, P., and Winguth, C.: A model-data comparison for a multi-model ensemble of early Eocene atmosphere–ocean simulations: EoMIP, Clim. Past, 8, 1717–1736, doi:10.5194/cp-8-1717-2012, 2012.

Murakami, S., Ohgaito, R., Abe-Ouchi, A., Crucifix, M., and Otto-Bliesner, B. L.: Global-scale energy and freshwater balance in glacial climate: a comparison of three PMIP2 LGM simulations, J. Climate, 21, 5008–5033, 2008.

Raymo, M. E., Grant, B., Horowitz, M., and Rau, G. H.: Mid-Pliocene warmth: Stronger greenhouse and stronger conveyor, Mar. Micropalaeontol., 27, 313–326, 1996.

Salzmann, U., Haywood, A. M., Lunt, D. J., Valdes, P. J., and Hill, D. J.: A new global biome reconstruction and data-model comparison for the Middle Pliocene, Global Ecol. Biogeogr., 17, 432–447, 2008.

Salzmann, U., Dolan, A. M., Haywood, A. M., Chan, W- L., Hill, D. J., Abe-Ouchi, A., Otto-Bliesner, B. L., Bragg, F. J., Chandler, M. A., Contoux, C., Jost, A., Kamae, Y., Lohmann, G., Lunt, D. J., Pickering, S. J., Pound, M. J., Ramstein, G., Rosenbloom, N. A., Sohl, L.,

Stepanek, C., Ueda, H., and Zhang, Z.: How well do models reproduce warm terrestrial climates of the Pliocene?, Nature Climate Change, in review, 2013.

Seki, O., Foster, G. L., Schmidt, D. N., Mackensen, A., Kawamura, K., and Pancost, R. D.: Alkenone and boron based Pliocene pCO_2 records, Earth Planet. Sci. Lett., 292, 201–211, doi:10.1016/j.epsl.2010.01.037, 2010.

Sloan, L. C., Crowley, T. J., and Pollard, D.: Modeling of middle Pliocene climate with the NCAR GENESIS general circulation model, Mar. Micropaleontol., 27, 51–61, 1996.

Sohl, L. E., Chandler, M. A., Schmunk, R. B., Mankoff, K., Jonas, J. A., Foley, K. M., and Dowsett, H. J.: PRISM3/GISS topographic reconstruction, US Geol. Surv. Data Series 419, Reston, Virginia, 2009.

Stepanek, C. and Lohmann, G.: Modelling mid-Pliocene climate with COSMOS, Geosci. Model Dev., 5, 1221–1243, doi:10.5194/gmd-5-1221-2012, 2012.

Yang, S.-K. and Smith, G. L.: Further studies on atmospheric lapse rate regimes, J. Atmos. Sci., 42, 961–965, 1985.

Zhang, R., Yan, Q., Zhang, Z. S., Jiang, D., Otto-Bliesner, B. L., Haywood, A. M., Hill, D. J., Dolan, A. M., Stepanek, C., Lohmann, G., Contoux, C., Bragg, F., Chan, W.-L., Chandler, M. A., Jost, A., Kamae, Y., Abe-Ouchi, A., Ramstein, G., Rosenbloom, N. A., Sohl, L., and Ueda, H.: East Asian monsoon climate simulated in the PlioMIP, Clim. Past Discuss., 9, 1135–1164, doi:10.5194/cpd-9-1135-2013, 2013.

Zhang, Z. S., Nisancioglu, K., Bentsen, M., Tjiputra, J., Bethke, I., Yan, Q., Risebrobakken, B., Andersson, C., and Jansen, E.: Pre-industrial and mid-Pliocene simulations with NorESM-L, Geosci. Model Dev., 5, 523–533, doi:10.5194/gmd-5-523-2012, 2012.

Zhang, Z. S., Nisancioglu, K. H., and Ninnemann, U. S.: Increased ventilation of Antarctic deep water during the warm mid-Pliocene, Nat. Commun., 4, 1499, doi:10.1038/ncomms2521, 2013a.

Zhang, Z.-S., Nisancioglu, K. H., Chandler, M. A., Haywood, A. M., Otto-Bliesner, B. L., Ramstein, G., Stepanek, C., Abe-Ouchi, A., Chan, W.-L., Bragg, F. J., Contoux, C., Dolan, A. M., Hill, D. J., Jost, A., Kamae, Y., Lohmann, G., Lunt, D. J., Rosenbloom, N. A., Sohl, L. E., and Ueda, H.: Mid-pliocene Atlantic meridional overturning circulation not unlike modern?, Clim. Past Discuss., 9, 1297–1319, doi:10.5194/cpd-9-1297-2013, 2013b.

Table 1. Key model and experimental design parameters for each of the eight PlioMIP Experiment 2 simulations.

GCM	Atmospheric Resolution (° lat × ° long × levels)	Ocean Resolution (° lat × ° long × levels)	Boundary Conditions Employed	Ocean Initialization	Reference
CCSM4	0.9 × 1.25 × 26	1 × 1 × 60	Alternate	PRISM3 (anomaly)	Rosenbloom et al. (2013)
COSMOS	3.75 × 3.75 × 19	3 × 1.8 × 40	Preferred	PRISM3 (anomaly)	Stepanek and Lohmann (2012)
GISS-E2-R	2 × 2.5 × 40	1 × 1.25 × 32	Preferred	PRISM3	Chandler et al. (2013)
HadCM3	2.5 × 3.75 × 19	1.25 × 1.25 × 20	Alternate	PRISM2 mPWP control	Bragg et al. (2012)
IPSLCM5A	3.75 × 1.9 × 39	0.5–2 × 2 × 31	Alternate	Pre-industrial control	Contoux et al. (2012)
MIROC4m	2.8 × 2.8 × 20	0.5–1.4 × 1.4 × 43	Preferred	PRISM3	Chan et al. (2011)
MRI-CGCM 2.3	2.8 × 2.8 × 30	0.5–2 × 2.5 × 23	Alternate	PRISM3 (anomaly)	Kamae and Ueda (2012)
NorESM-L	3.75 × 3.75 × 26	3 × 3 × 30	Alternate	Levitus	Zhang et al. (2012)

Table 2. The climate sensitivity and global mean annual surface air temperature warming of each of the models with simulations in PlioMIP Experiment 2 ensemble. Climate sensitivity is a general value for each model and does not refer to the particular set up and initialization procedures used for PlioMIP.

GCM	Climate Sensitivity (°C)	Mean Annual mPWP SAT Warming (°C)
CCSM4	3.2	1.86
COSMOS	4.1	3.60
GISS-E2-R	2.7	2.24
HadCM3	3.1	3.27
IPSLCM5A	3.4	2.03
MIROC4m	4.1	3.46
MRI-CGCM 2.3	3.2	1.84
NorESM-L	3.1	3.27

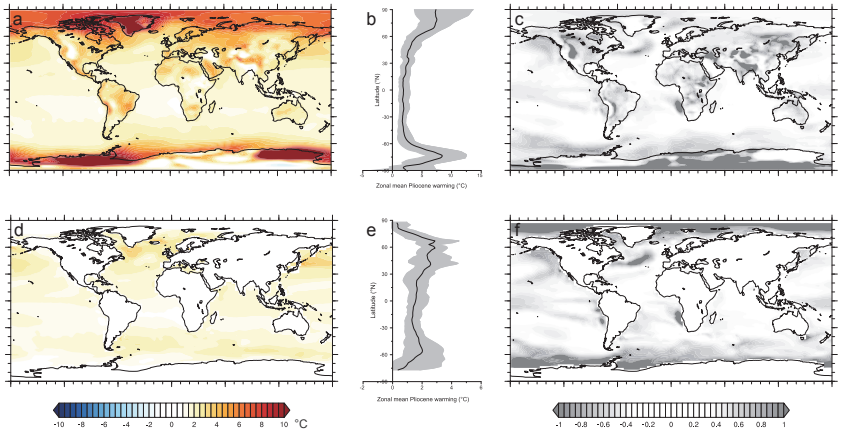

Fig. 1. Multi-model mean PlioMIP Experiment 2 warming between mid-Pliocene and pre-industrial simulations. **(a)** Annual mean surface air temperature (SAT) warming, **(b)** zonal mean SAT warming (solid line), with shading showing the range of model simulations, and **(c)** relative variance between the PlioMIP Experiment 2 simulations (σ/ΔSAT). **(d)** Annual mean sea surface temperature (SST) warming, **(e)** zonal mean SST warming and **(f)** relative variance of SSTs.

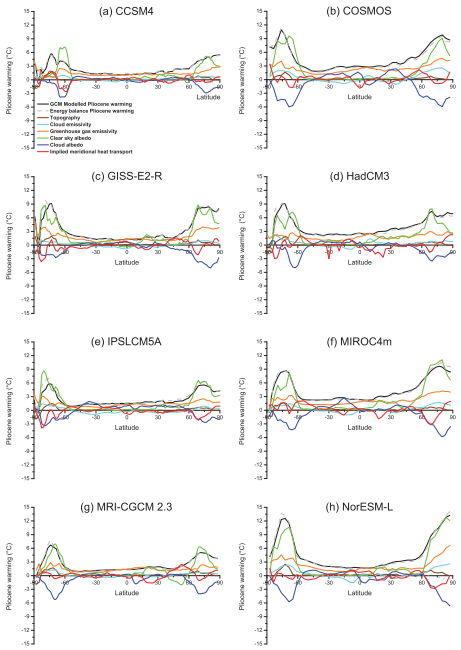

Fig. 2. Energy balance analysis for each of the eight PlioMIP Experiment 2 simulations, from **(a)** CCSM4, **(b)** COSMOS, **(c)** GISS-E2-R, **(d)** HadCM3, **(e)** IPSLCM5A, **(f)** MIROC4m, **(g)** MRI-CGCM 2.3 and **(f)** NorESM-L. Plots show the zonal mean warming, at each latitude in the model, from each of the energy balance components. Solid black line is the zonal mean surface air temperature increase from the GCM simulation, while the dashed grey line is the Pliocene warming approximated by the energy balance calculations.

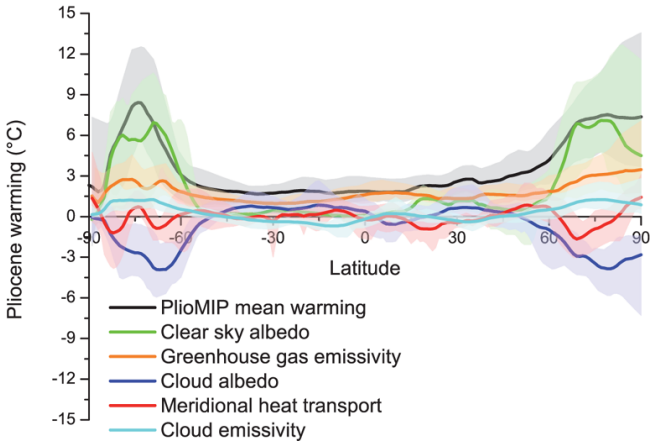

Fig. 3. Summary of the PlioMIP Experiment 2 energy balance analysis. Solid line shows the multi-model mean warming for each component, with the associated shading representing the range. These values have been interpolated onto a 1° latitude grid for comparison purposes.

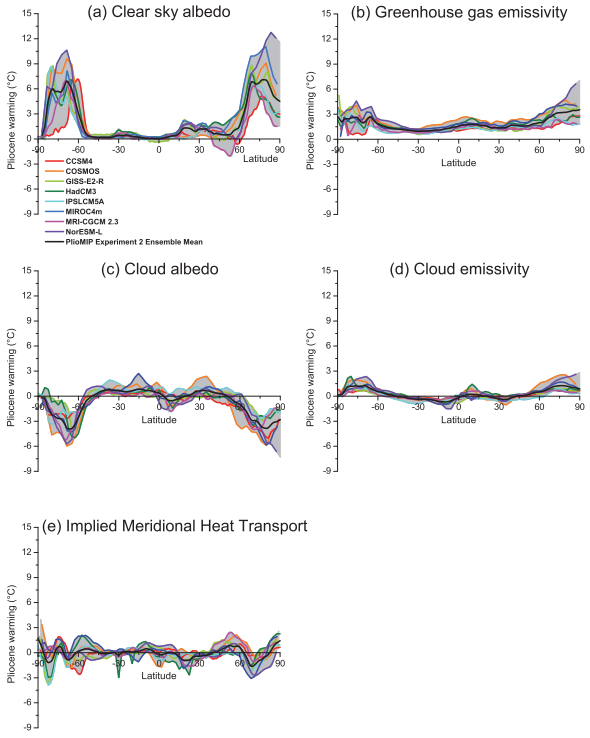

Fig. 4. Breakdown of the energy balance components, **(a)** clear sky albedo, **(b)** greenhouse gas emissivity, **(c)** cloud albedo, **(d)** cloud emissivity and **(e)** implied meridional heat transport. Solid black line shows the multi-model mean, range is shown by the grey shading and each of the individual model results is shown by the coloured solid lines.

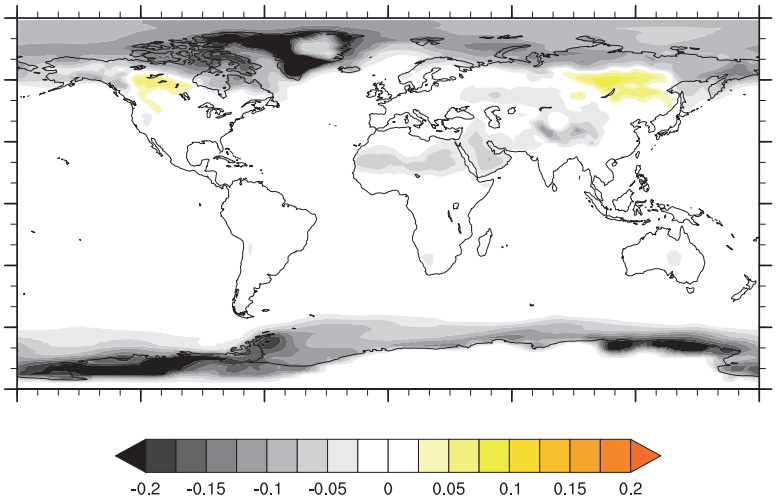

Fig. 5. Spatial distribution of multi-model mean changes in the clear sky albedo between mid-Pliocene and pre-industrial simulations. This primarily shows changes due to specified vegetation and global ice sheets and modelled sea ice and snow cover, although it includes an atmospheric component. Greyscale shows reductions in albedo, generally associated with warming and yellow shading indicates increases in albedo that would generally cause a reduction surface air temperature.